

Article

Analytical–Numerical Solution for the Skin and Proximity Effects in Two Parallel Round Conductors

Paweł Jabłoński ^{1,*}, Tomasz Szczegielniak ², Dariusz Kusiak ¹ and Zygmunt Piątek ²

¹ Institute of Optoelectronics and Measurement Systems, Faculty of Electrical Engineering, Czestochowa University of Technology, Armii Krajowej 17, 42-200 Czestochowa, Poland; d.kusiak@el.pcz.czest.pl

² Institute of Environmental Engineering, Faculty of Infrastructure and Environment, Czestochowa University of Technology, Brzeźnicka St. 60a, 42-200 Czestochowa, Poland; tszczegielniak@is.pcz.pl (T.S.); zygmunt.piatek@interia.pl (Z.P.)

* Correspondence: p.jablonski@el.pcz.czest.pl; Tel.: +48-34-325-0306

Received: 30 July 2019; Accepted: 16 September 2019; Published: 19 September 2019



Abstract: This paper describes an analytical-numerical method for the skin and proximity effects in a system of two parallel conductors of circular cross section—a system very frequently encountered in various applications. The magnetic field generated by the current applied on each conductor is expressed by means of vector magnetic potential and expanded into Fourier series. Using the Laplace and Helmholtz equations, as well as the classical boundary conditions, the current density induced due to the proximity and skin effect is determined in each conductor. The resulting current density is expressed as a series of successive reactions. The results obtained are compared with those obtained via finite elements. Although the paper is theoretical, the considered problem has a practical significance, because transmission lines with round conductors are universally used. Besides, the results can be used to estimate errors when only the first reaction is taken into account, which gives relatively simple formulas.

Keywords: skin effect; proximity effect; cylindrical conductors; current density; successive approximations

1. Introduction

A system of two or more wires of circular cross section (cylindrical wires, briefly called round wires) is very often used in power and signal transmission lines. For example, in a three phase cable line, there are three round wires arranged into a three-core cable or three single-core cables in the trefoil or flat formation [1]. In each conductor, eddy currents are induced by a magnetic field generated by the current in the wire itself (skin effect), as well as by the neighboring alternating phase currents (proximity effect). These currents add to the applied currents. Consequently, the total current densities in conductors become non-uniform and non-symmetrical, and significantly affect the electromagnetic field, power losses in the wires, and the impedance matrix of such a system of conductors [2–5]. Thus, the knowledge on the current density distribution is essential in determining the network properties of such lines.

Throughout the last 150 years, since Maxwell’s formulation of the electromagnetic field equations, the proximity effect in parallel conductors with sinusoidal currents has been investigated by many researchers who have proposed a variety of methods to calculate the current density inside wires and/or their impedance. In general, the methods use differential or integral formulation. The first requires solving the Helmholtz equation in the conductive regions, and the Laplace equation in the surrounding region, whereas the second leads to integral equation(s). Excluding coaxial cables, a purely analytical approach to obtain exact solution in both formulations encounters mathematical problems. For example, the method of separation of variables for two identical round wires cannot

be used, because the variables in the Helmholtz equation in bipolar coordinates cannot be separated. The situation is even worse for other shapes of wire cross sections, or in case of multiple wires. To overcome these problems a variety of approximate approaches are used, like:

- Introducing significant simplifications—the most radical simplification is a configuration of two extensive plates (often encountered in academic handbooks to illustrate the proximity effect); much more sophisticated is substituting some wires with filaments (e.g., [6–10]).
- Using approximate analytical expressions—e.g., various approximate formulas for alternating current resistance can be found in [11–13] and approximations for inductances are given in [14]; integral equation with current density approximated with finite power series was proposed in [15,16]; multipole expansion with finite number of terms was used in [17].
- Using numerical methods, like finite elements (e.g., [5,18,19]), boundary elements (e.g., [20]), FDTD [21], solving the Fredholm equation with various basis functions (e.g., [22,23]), and others.
- Mixing analytical and numerical methods—e.g., Rolicz proposed solving the problem with the Bubnov–Galerkin method in the wires and the method of separation of variables in the surrounding region [24].
- Representing the conductors as multiple wires of “small” cross sections and connected in parallel—e.g., [2,4,25,26].

The above classification is not meant to be complete, but it shows that the investigations on the proximity effect are still up to date. From the scientific point of view, the most valuable are simple analytical solutions. Such an approach is shown, among others, in [7,8], where the neighboring round wires are considered as current filaments. This paper can be regarded as an extension the mentioned works. The idea is to represent the neighboring wire not with a single filament, but with a set of filaments rather, similarly as in [26]. This makes it possible to take into account the reverse reaction of the induced eddy currents, keeping analytical form of the solution. It is worth emphasizing that in contrary to many methods described in the literature, the proposed approach does not require numerical solving of any system of algebraic equations.

2. Methodology

2.1. The Idea of the Method

Let us start with the geometry shown in Figure 1, where two infinitely long parallel conductors of circular cross sections are shown. The radii of the conductors are R_1 and R_2 , respectively, and the distance between the conductor axes is d . A sinusoidal current of angular frequency ω and complex root mean square (r.m.s.) value I_1 flows through the first conductor (on the right).

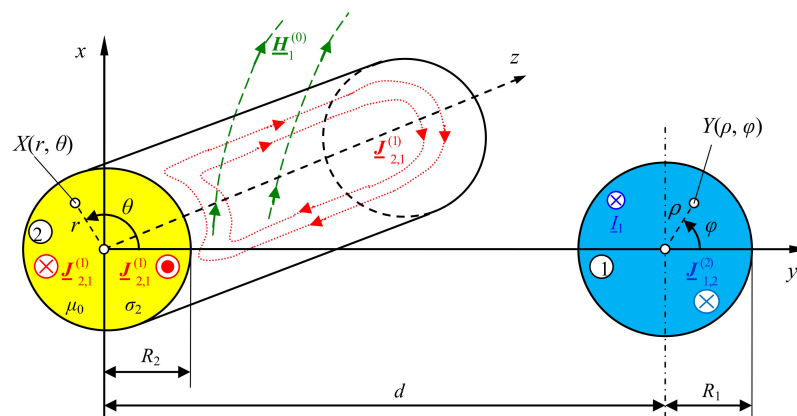


Figure 1. Current I_1 induces eddy currents of density $J_{2,1}^{(1)}$ in the left conductor, which in turn generates eddy currents $J_{1,2}^{(2)}$ in the right conductor.

Suppose the current has a density of $\underline{J}_1^{(0)}$, where (0) in the superscript indicates the 0th approximation. This current generates a time harmonic magnetic field $\underline{H}_1^{(0)}$, which induces eddy currents of density $\underline{J}_{2,1}^{(1)}$ in the second conductor (on the left). This current is a secondary source of magnetic field $\underline{H}_{2,1}^{(1)}$, which in turn induces eddy currents $\underline{J}_{1,2}^{(2)}$ in the first conductor. This sequence of successive reactions can be continued, but in practice, the next reactions can often be neglected.

In [7,8], the current in the first conductor, I_1 , was assumed to be located at the axis of wire 1 as a filament current. The magnetic field generated by it was expressed in terms of magnetic vector potential in the form of power series. In the non-conducting region outside the second conductor, the Laplace equation was used, taking into account the reverse reaction of the eddy currents induced in the considered conductor. Inside the conductor, the Helmholtz equation for the eddy current density was used and supplemented with classical continuity conditions. The solutions obtained were used to determine the total eddy current density induced in the first conductor, as well as in the second one. The essential Equations describing the approach are given below. It is convenient to introduce a coordinate system with a z -axis along the axis of the left wire. Due to assumed infinite length of the conductors and their fixed cross section, the fields are independent on z coordinate. Moreover, current density only has a z -component, ($\underline{J} = J\hat{z}$). The current density in conductor 2, induced by current I_1 concentrated in a filament located on the axis of wire 1, can be expressed as follows (see Equation (A18) in Appendix A for details):

$$\underline{J}_{2,1}^{(1)}(r, \theta) = -\frac{I_1}{\pi R_2^2} \underline{\Gamma}_2 R_2 \sum_{n=1}^{\infty} \left(\frac{R_2}{d}\right)^n \frac{I_n(\underline{\Gamma}_2 r)}{I_{n-1}(\underline{\Gamma}_2 R_2)} \cos n\theta \quad (1a)$$

in which $I_n(x)$ is the modified Bessel function of the first kind of orders n , and

$$\underline{\Gamma}_2 = \sqrt{j\omega\mu_2\sigma_2} = \frac{1+j}{\delta_2}, \quad (1b)$$

where σ_2 and μ_2 are the electric conductivity and magnetic permeability of wire 2, respectively, $\delta_2 = \sqrt{2/\omega\mu_2\sigma_2}$ is the skin depth in wire 2, and $j = \sqrt{-1}$ is the imaginary unit.

By interchanging the roles of the conductors, it is easy to obtain the current density in conductor 2, induced by current I_2 concentrated in filament located on the axis of wire 2:

$$\underline{J}_{1,2}^{(1)}(\rho, \varphi) = -\frac{I_2}{\pi R_1^2} \underline{\Gamma}_1 R_1 \sum_{n=1}^{\infty} (-1)^n \left(\frac{R_1}{d}\right)^n \frac{I_n(\underline{\Gamma}_1 \rho)}{I_{n-1}(\underline{\Gamma}_1 R_1)} \cos n\varphi \quad (2a)$$

with

$$\underline{\Gamma}_1 = \sqrt{j\omega\mu_1\sigma_1}, \quad (2b)$$

where σ_1 is the electric conductivity of wire 1, and μ_1 is the magnetic permeability of wire 1.

However, it should be realized that the eddy currents of density given by Equation (1a) induce eddy currents of density $\underline{J}_{1,2}^{(2)}(\rho, \varphi)$ in the first conductor, which in turn induce eddy currents $\underline{J}_{2,1}^{(3)}(r, \theta)$ in wire 2, and so forth. Similarly, eddy currents of density given by Equation (2a) induce currents $\underline{J}_{2,1}^{(2)}(r, \theta)$ in conductor 2, and so on. Hence, the total current density in the second conductor can be regarded as the following sum:

$$\underline{J}_2(r, \theta) = \underline{J}_2^{(0)}(r, \theta) + \sum_{m=1}^{\infty} \underline{J}_{2,1}^{(m)}(r, \theta). \quad (3a)$$

In practice, it is usually necessary to cut the infinite series at certain M as follows:

$$J_2^{[M]}(r, \theta) = J_2^{(0)}(r, \theta) + \sum_{m=1}^M J_{2,1}^{(m)}(r, \theta). \quad (3b)$$

where in this work $[M]$ in the superscript is used to indicate the series cut at M th term.

Similar Equations can be written for wire 1. In previous works, e.g., [7,8], the stress was put on $J_{2,1}^{(1)}(r, \theta)$ and $J_{2,1}^{[1]}(r, \theta)$ with I_1 focused on the axis of wire 1, whereas in this paper the reactions of higher order are considered. Of course, such an approach is somewhat artificial, because none of the successive reactions exists alone; thus, they cannot be measured. The method should be regarded as a certain way of calculating the total current density distribution. It can be used, for example, to estimate how the higher reactions affect the results obtained from the lowest ones.

2.2. The Skin Effect as the Initial Approximation

In approximation 0, it is assumed that the current is distributed as if the wires were standalone with the skin effect taken into account. The well-known Equation for the current density in a long straight cylindrical wire with time harmonic current leads to the following result for wire 1 [27]:

$$J_1^{[0]}(\rho, \varphi) = J_1^{(0)}(\rho, \varphi) = \frac{I_1}{\pi R_1^2} \frac{\Gamma_1 R_1}{2} \frac{I_0(\Gamma_1 \rho)}{I_1(\Gamma_1 R_1)}. \quad (4a)$$

Similarly, the following Equation can be written for wire 2:

$$J_2^{[0]}(r, \theta) = J_2^{(0)}(r, \theta) = \frac{I_2}{\pi R_2^2} \frac{\Gamma_2 R_2}{2} \frac{I_0(\Gamma_2 \rho)}{I_1(\Gamma_2 R_2)}. \quad (4b)$$

2.3. The First Correction Due to the Proximity Effect

In Equations (4a) and (4b), the skin effect is taken into account, but the proximity effect is neglected. The next step is to take into account the first correction related with the proximity effect. In terms of the notation used in the paper, this correction for wire 2 is denoted as $J_{2,1}^{(1)}$, and it is generated by $J_1^{(0)}$. In general, to take into account the non-uniform distribution of $J_1^{(0)}$, a set of substitutive filaments with suitable currents can be used. For example, they could be arranged in a polar grid. However, this is not necessary in the case of cylindrical wires, because a standalone straight cylindrical wire with current flowing along it generates the same field outside as if the current was focused in a filament on the axis of the wire, and the skin effect does not matter. This is a well-known result and can be easily found from the Ampère law or by direct integration. Mathematically, it results from cylindrical symmetry, which makes the equations independent on the angular coordinate. Therefore, although the skin effect in the source wire may seem neglected, the eddy currents induced in the neighboring conductor and given by Equations (1a) and (2a) take into account the skin effect in the source conductor. Hence, up to the first reaction, the current density distribution in wire 2 is as follows:

$$J_2^{[1]}(r, \theta) = J_2^{(0)}(r, \theta) + J_{2,1}^{(1)}(r, \theta). \quad (5)$$

A similar equation can be written for wire 1. Typically, two cases are often considered: Same currents ($I_2 = I_1 = I$) and opposing currents ($I_2 = -I_1 = -I$). This leads to the following equations, taking into account the skin effect and the first approximation of the proximity effect:

$$J_1^{[1]}(\rho, \varphi) = \frac{I}{\pi R_1^2} \left(\frac{\Gamma_1 R_1}{2} \frac{I_0(\Gamma_1 \rho)}{I_1(\Gamma_1 R_1)} \mp \Gamma_1 R_1 \sum_{n=1}^{\infty} (-1)^n \left(\frac{R_1}{d} \right)^n \frac{I_n(\Gamma_1 \rho)}{I_{n-1}(\Gamma_1 R_1)} \cos n\varphi \right), \quad (6a)$$

$$J_2^{[1]}(r, \theta) = \pm \frac{I}{\pi R_2^2} \left(\frac{\Gamma_2 R_2}{2} \frac{I_0(\Gamma_2 \rho)}{I_1(\Gamma_2 R_2)} \mp \Gamma_2 R_2 \sum_{n=1}^{\infty} \left(\frac{R_2}{d} \right)^n \frac{I_n(\Gamma_2 r)}{I_{n-1}(\Gamma_2 R_2)} \cos n\theta \right), \tag{6b}$$

where the upper and lower signs are for the same and opposing currents, respectively.

2.4. The Second Approximation

As mentioned in Section 2, eddy current of density $J_{2,1}^{(1)}(r, \theta)$ generates its own magnetic field which induces additional eddy currents in wire 1, denoted as $J_{1,2}^{(2)}(\rho, \varphi)$. Let us consider an elementary fragment of cross section of wire 2. The current associated with it, due to the first approximation of the proximity effect, equals $J_{2,1}^{(1)}(r, \theta)rdrd\theta$ and generates magnetic vector potential at point $Y(\rho, \varphi)$ as follows:

$$dA_{2,1}^{(1)}(Y; X) = \frac{\mu_0 J_{2,1}^{(1)}(r, \theta)rdrd\theta}{2\pi} \ln \frac{1}{|X - Y|} + const, \tag{7a}$$

where $X(r, \theta)$ is arbitrary point in wire 2. Thus the total magnetic potential due to $J_{2,1}^{(1)}(r, \theta)$ equals

$$A_{1,2}^{(1)}(Y; X) = \iint_{(r, \theta)} dA_{2,1}^{(1)}(Y(r, \varphi); X(\rho, \theta)) = \int_{r=0}^{R_2} \int_{\theta=0}^{2\pi} \frac{\mu_0 J_{2,1}^{(1)}(r, \theta)}{2\pi} \ln \frac{1}{|X - Y|} rdrd\theta + const. \tag{7b}$$

To evaluate the integral, it is proposed to divide the cross section of wire 2 into circular sectors and represent the integral as a sum of integrals over the sectors. At this moment, the details of the sectors are not important—they are described in Section 2.5. If the sectors are small enough, the integrand may be assumed constant so that

$$A_{1,2}^{(1)} \approx \sum_{s=1}^S \frac{\mu_0 J_{2,1}^{(1)}(r, \theta)}{2\pi} \ln \frac{1}{|X - Y|} \Delta S_s + const, \tag{7c}$$

where S is the number of sectors and ΔS_s is the area of sector s . If $2\Delta r_s$ and $2\Delta \theta_s$ are the radial and angular dimensions of the sector, respectively, then

$$\Delta S_s = r_s \Delta r_s \Delta \theta_s. \tag{8a}$$

In this way, current density $J_{2,1}^{(1)}(r, \theta)$ in wire 2 is represented as a set of filaments with currents

$$I_{2,1,s}^{(1)} = J_{2,1}^{(1)}(r_s, \theta_s) \Delta S_s, \tag{8b}$$

where (r_s, θ_s) are polar coordinates of the sector center. Thus, Equation (7c) can be rewritten as follows:

$$A_{1,2}^{(1)}(\rho, \varphi) \approx \frac{\mu_0}{2\pi} \sum_{s=1}^S I_{2,1,s}^{(1)} \ln \frac{1}{|X(\rho, \varphi) - Y(r_s, \theta_s)|} + const. \tag{9}$$

Using Equation (A18) from Appendix A for each filament leads to the following expression for eddy currents induced in wire 1 due to potential $A_{1,2}^{(1)}(\rho, \varphi)$:

$$J_{1,2}^{(2)}(\rho, \varphi) = -\frac{1}{\pi R_1^2} \Gamma_1 R_1 \sum_{s=1}^S I_{2,1,s}^{(1)} \sum_{\xi_s=1}^{\infty} \left(\frac{R_1}{\xi_s} \right)^n \frac{I_n(\Gamma_1 \rho)}{I_{n-1}(\Gamma_1 R_1)} \cos n(\pi - \varphi - \psi_s), \tag{10}$$

where by the cosine theorem (see Figure 2), it follows that

$$\xi_s = \sqrt{r_s^2 + d^2 - 2r_s d \cos \theta_s} \tag{11a}$$

and

$$\psi_s = \arcsin \frac{r_s \sin \theta_s}{\xi_s}. \tag{11b}$$

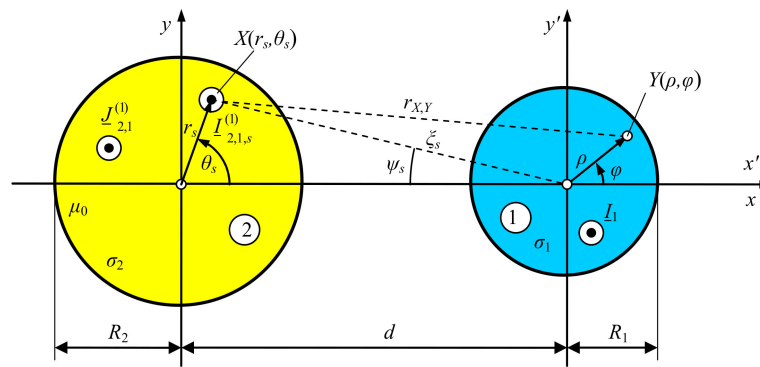


Figure 2. Relationships between polar coordinates (r_s, θ_s) related to current filament located in the center of sector s in wire 2 and polar coordinates (ρ, φ) related to wire 1.

In a similar way, the second approximation for the eddy currents in wire 2 due to the proximity effect can be found. Based on Equation (10), and interchanging the roles of the wires, it is easy to write the following equation:

$$J_{2,1}^{(2)}(r, \theta) = -\frac{1}{\pi R_2^2} \Gamma_2 R_2 \sum_{v=1}^V I_{1,2,v}^{(1)} \sum_{n=1}^{\infty} \left(\frac{R_2}{\xi_v}\right)^n \frac{I_n(\Gamma_2 r)}{I_{n-1}(\Gamma_2 R_2)} \cos n(\theta - \psi_v), \tag{12}$$

where V is the number of sectors in wire 1, subscript $v = 1, 2, \dots, V$ refers to sector v in that wire, and (see Figure 3):

$$I_{1,2,v}^{(1)} = I_{1,2}^{(1)}(\rho_v, \varphi_v) \Delta S_v, \tag{13a}$$

$$\xi_v = \sqrt{\rho_v^2 + d^2 + 2\rho_v d \cos \varphi_v}, \tag{13b}$$

$$\psi_v = \arcsin \frac{\rho_v \sin \varphi_v}{\xi_v}. \tag{13c}$$

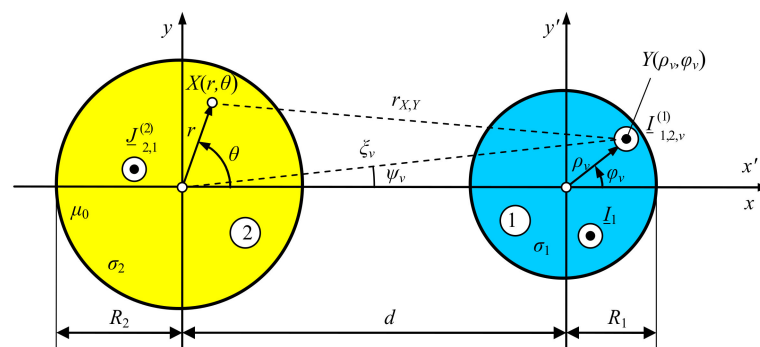


Figure 3. Relationships between polar coordinates (ρ_v, φ_v) related to current filament located in wire 1 and polar coordinates (r, θ) related to wire 2.

2.5. Discretization of Wires

At this moment, it is worth saying something more on the division of wires into sectors. It can be done in an arbitrary way, but the sectors should cover the entire wire cross section and their size should be significantly smaller than the skin depth. Two choices based on polar grid are shown in Figure 4. The first possibility uses sectors arranged in a regular polar grid (Figure 4a). If the radius is divided into P sections, and the full angle is divided into T sections, then the total number of sectors will be $S = PT$. The sector sizes are $\Delta r_s = R_2/P$ and $\Delta\theta_s = 2\pi/T$, and the sector centers have polar coordinates $(r_p, \theta_t) = \left(\frac{2p-1}{2}\Delta r_s, (t-1)\Delta\theta_s\right)$, where $p = 1, 2, \dots, P$ and $t = 1, 2 \dots, T$. This division is simple, but the sectors near the surface of the wire are much larger than those near the center. To keep accuracy, it is necessary to take a large enough T so that the most outer sectors are not too large. Hence, the filaments near the center will be distributed very densely, which will require much unnecessary computational effort in further calculations.

One way to avoid the above-mentioned inconvenience is using a polar grid with the number of angular sections, T_p , proportional to the radius (Figure 4b). It is reasonable to use square-like sectors. Hence, from desired equity $2\pi r_p/T_p = \Delta r_s$, it follows that the number of angular segments on circle $r = r_p$ should be equal to $(2p-1)\pi$ (or rather, an integer closest to this value). In practice, it could be more desirable to use $T_p = 4(2P-1)$, because then the sectors are distributed with nice symmetry. In such a case, the total number of sectors will be $S = \sum_{p=1}^P T_p = 4P^2$. When compared with the regular grid with $T = 4(2P-1)$ sectors per ring, it follows that the number of sectors in the second case is about two times smaller than in the first one ($\frac{4P^2}{P4(2P-1)} \approx 0.5$). This gives significantly less computational effort, keeping the accuracy at the same level.

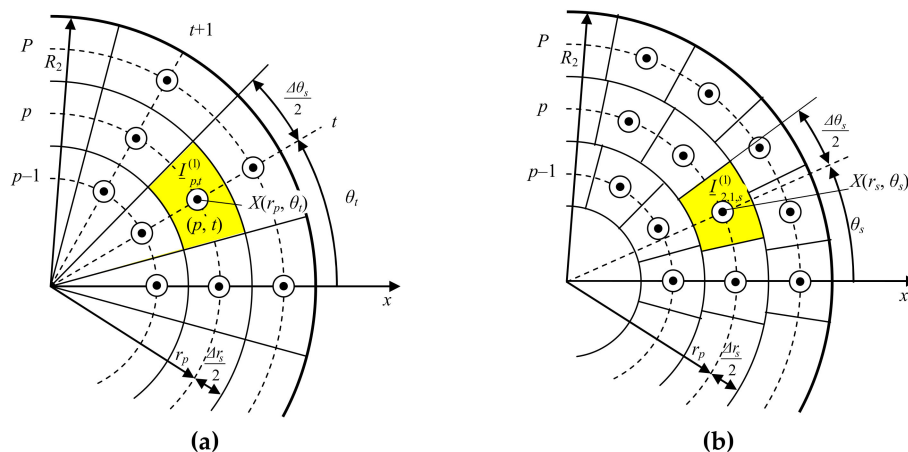


Figure 4. Divisions of wire 2 into sectors based on polar grids: (a) Regular division into P rings and T sectors within each ring; (b) division into P rings and variable number of sectors within each ring.

2.6. Higher Order Reactions

In a similar way, the next reactions can be determined. Given $J_{1,2}^{(m)}(\rho, \varphi)$, reaction $m + 1$ can be found. Based on Equations (12) and (13), one can write

$$J_{2,1}^{(m+1)}(r, \theta) = -\frac{1}{\pi R_2^2} \Gamma_2 R_2 \sum_{v=1}^V I_{1,2,v}^{(m)} \sum_{n=1}^{\infty} \left(\frac{R_2}{\xi_v}\right)^n \frac{I_n(\Gamma_2 r)}{I_{n-1}(\Gamma_2 R_2)} \cos n(\theta - \psi_v), \quad (14a)$$

where

$$I_{1,2,v}^{(m)} = I_{1,2}^{(m)}(\rho_v, \varphi_v) \Delta S_v. \quad (14b)$$

By analogy, given $\underline{J}_{2,1}^{(m)}(r, \theta)$ one obtains

$$\underline{J}_{1,2}^{(m+1)}(\rho, \varphi) = -\frac{1}{\pi R_1^2} \underline{I}_1 R_1 \sum_{s=1}^S \underline{I}_{2,1,s}^{(m)} \sum_{n=1}^{\infty} \left(\frac{R_1}{\xi_s}\right)^n \frac{I_n(\underline{I}_1 \rho)}{I_{n-1}(\underline{I}_1 R_1)} \cos n(\pi - \varphi - \psi_s), \tag{15a}$$

where

$$\underline{I}_{2,1,s}^{(m)} = \underline{J}_{2,1}^{(m)}(r_s, \theta_s) \Delta S_s. \tag{15b}$$

To simplify and shorten the notation of the above Equations for successive reactions, it is worth introducing the following auxiliary function:

$$\Lambda\left(\frac{r}{R}, \theta, \frac{R}{d}, \underline{I}R\right) = -\underline{I}R \sum_{n=1}^{\infty} \left(\frac{R}{d}\right)^n \frac{I_n(\underline{I}R \frac{r}{R})}{I_{n-1}(\underline{I}R)} \cos n\theta. \tag{16}$$

It represents the eddy current density in units of $\underline{I}/\pi R^2$ induced in a cylindrical wire of radius R and the skin effect parameter $\underline{I} = (1 + j)/\delta$ (where δ is the skin depth) due to parallel current filament \underline{I} located at a distance of $d > R$ from the wire axis (see geometry shown in Figure A1). Then Equations (1a), (2a), (14a) and (15a) can be rewritten as follows:

$$\underline{J}_{2,1}^{(1)}(r, \theta) = \frac{\underline{I}_1}{\pi R_2^2} \Lambda\left(\frac{r}{R_2}, \theta, \frac{R_2}{d}, \underline{I}_2 R_2\right), \tag{17a}$$

$$\underline{J}_{1,2}^{(1)}(\rho, \varphi) = \frac{\underline{I}_2}{\pi R_1^2} \Lambda\left(\frac{\rho}{R_1}, \pi - \varphi, \frac{R_1}{d}, \underline{I}_1 R_1\right), \tag{17b}$$

$$\underline{J}_{2,1}^{(m+1)}(r, \theta) = \frac{1}{\pi R_2^2} \sum_{v=1}^V \underline{I}_{1,2,v}^{(m)} \Lambda\left(\frac{r}{R_2}, \theta - \psi_v, \frac{R_2}{\xi_v}, \underline{I}_2 R_2\right), \tag{17c}$$

$$\underline{J}_{1,2}^{(m+1)}(\rho, \varphi) = \frac{1}{\pi R_1^2} \sum_{s=1}^S \underline{I}_{2,1,s}^{(m)} \Lambda\left(\frac{\rho}{R_1}, \pi - \varphi - \psi_s, \frac{R_1}{\xi_s}, \underline{I}_1 R_1\right). \tag{17d}$$

2.7. Algorithm of Calculations

The algorithm of calculations is as follows:

1. Given $R_1, R_2, d, \sigma_1, \sigma_2, \omega, \underline{I}_1, \underline{I}_2$, calculate necessary values like $\underline{I}_1 R_1$ and $\underline{I}_2 R_2$.
2. Divide wires into sectors.
3. For $m = 1, 2, \dots, M - 1$ (where M is the number of reactions to be taken into account), calculate $\underline{I}_{2,1,s}^{(m)}$ and $\underline{I}_{1,2,v}^{(m)}$ using Equations (8b) + (17a), (13a) + (17b), (15b) + (17c), and (14b) + (17d).

This will produce currents in the sectors necessary to calculate all the corrections to the eddy current density due to proximity effect up to $\underline{J}_{1,2}^{(M)}$ and $\underline{J}_{2,1}^{(M)}$. It is worth noting that the procedure does not require solving any equation system. The successive reactions are calculated based on the previous one. It can be expected that the reactions of higher order can usually be neglected, unless the gap between the wires is very small.

To speed up numerical calculations, values of function $\Lambda(\dots)$ can be calculated after generating the sectors and before the main loop of calculating the successive reactions (step 2). This will produce two matrices, $\Lambda_{1,2;V \times S}$ and $\Lambda_{2,1;S \times V}$ of the following elements:

$$\Lambda_{1,2;v,s} = \frac{\Delta S_v}{\pi R_1^2} \Lambda\left(\frac{\rho_v}{R_1}, \pi - \varphi_v - \psi_s, \frac{R_1}{\xi_s}, \underline{I}_1 R_1\right), \tag{18a}$$

$$\Lambda_{2,1;s,v} = \frac{\Delta S_s}{\pi R_2^2} \Lambda \left(\frac{r_s}{R_2}, \theta_s - \psi_v, \frac{R_2}{\xi_v}, \Gamma_2 R_2 \right). \tag{18b}$$

It is also worth introducing two vectors, $\Lambda_{1:V \times 1}$ and $\Lambda_{2:S \times 1}$ the elements of which are

$$\Lambda_{1:v} = \frac{\Delta S_v}{\pi R_1^2} \Lambda \left(\frac{\rho_v}{R_1}, \varphi_v, \frac{R_1}{d}, \Gamma_1 R_1 \right), \tag{18c}$$

$$\Lambda_{2;s} = \frac{\Delta S_s}{\pi R_2^2} \Lambda \left(\frac{r_s}{R_2}, \theta_s, \frac{R_2}{d}, \Gamma_2 R_2 \right). \tag{18d}$$

The filament currents in wires 1 and 2, $I_{1,2;v}^{(m)}$ and $I_{2,1;s}^{(m)}$, can be arranged in two column vectors, $\mathbf{I}_{1,2:V \times 1}^{(m)}$ and $\mathbf{I}_{2,1:S \times 1}^{(m)}$, respectively. Thus, Equations (8b) + (17a), (13a) + (17b), (15b) + (17c), and (14b) + (17d) can be gathered and rewritten in matrix form as follows:

$$\mathbf{I}_{2,1}^{(m)} = \begin{cases} I_1 \Lambda_2 & \text{for } m = 1, \\ \Lambda_{2,1} \mathbf{I}_{1,2}^{(m-1)} & \text{for } m > 1, \end{cases} \tag{19a}$$

$$\mathbf{I}_{1,2}^{(m)} = \begin{cases} I_2 \Lambda_1 & \text{for } m = 1, \\ \Lambda_{1,2} \mathbf{I}_{2,1}^{(m-1)} & \text{for } m > 1, \end{cases} \tag{19b}$$

In this way, evaluating the successive reactions consists of multiplying the currents from the previous reaction by once generated matrices, which greatly speeds up the calculations.

3. Results and Discussion

3.1. Numerical Example

To illustrate the method, let us first consider two identical wires. To be more specific, let $R_1 = R_2 = 1$ mm, $d = 2.5$ mm (gap between the wires equal to 0.5 mm). The wires are from copper ($\sigma_1 = \sigma_2 = 55$ MS/m), and the frequency equals $f = 40$ kHz. Three cases are considered:

- Case 1: The current in wire 1 is non-zero and in wire 2 is zero;
- Case 2: The currents in both wires are the same; and
- Case 3: The currents in both wires are opposing.

The calculations are performed within the following values of operational parameters:

- Each wire is divided into $S = V = 100$ filaments ($P = 5$ with variable number of sections);
- The relative accuracy of Λ evaluation is $\epsilon = 10^{-3}$ (three meaningful digits—see Appendix B); and
- Six reactions were determined.

The discretization of the wires is shown in Figure 5. Figures 6 and 7 show the absolute value and argument of current density reactions on the surface of wire 1 and 2 in case 1. Reactions 0 to 6, as well as the total current density, are shown.

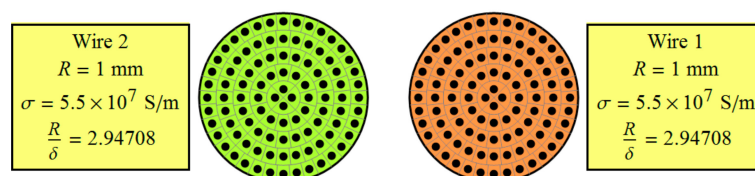


Figure 5. The view of the configuration under considerations (dots represent filaments).

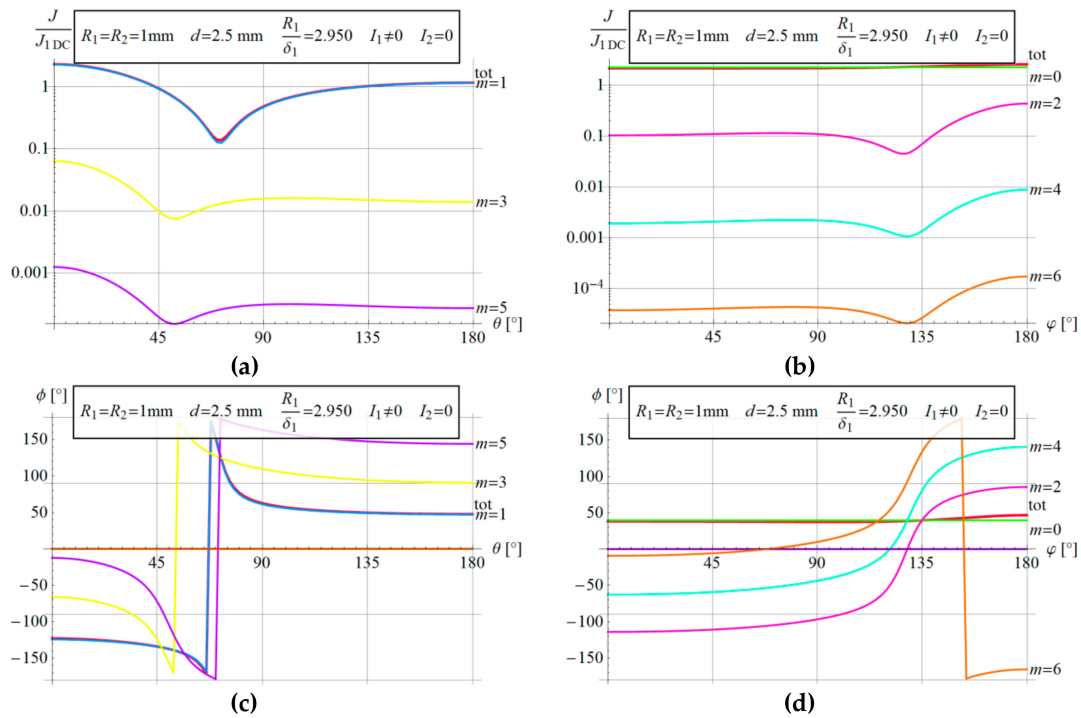


Figure 6. The successive reactions of eddy current density on the surfaces of the wires in case 1 (magnitudes of current density in units of $I_1/\pi R_1^2$, arguments ϕ of current density in degrees; legend: Red—total, green—skin effect, blue— $m = 1$, magenta— $m = 2$, yellow— $m = 3$, cyan— $m = 4$, violet— $m = 5$, orange— $m = 6$): (a) Current density magnitude in wire 2; (b) current density magnitude in wire 1; (c) current density argument in wire 2; (d) current density magnitude in wire 1.

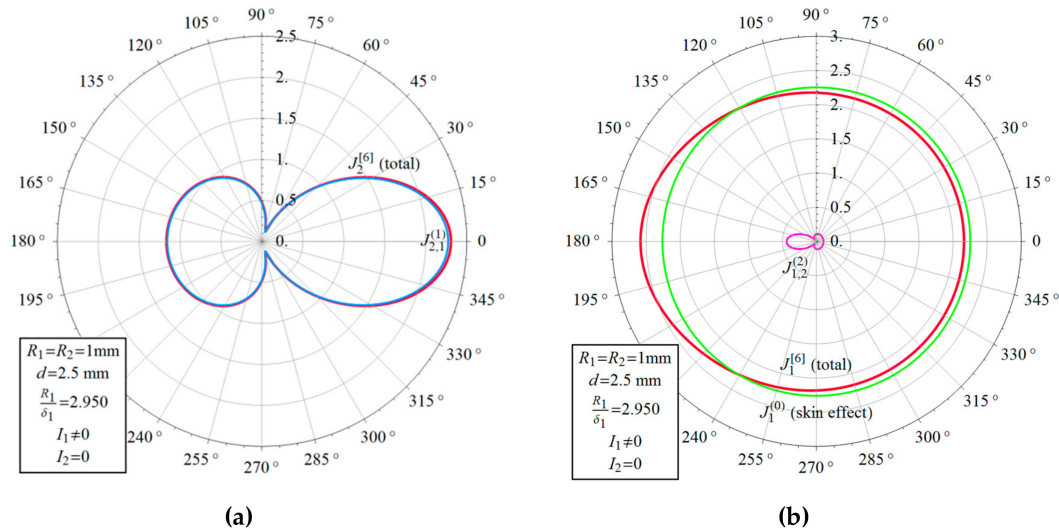


Figure 7. Polar plots of the successive reactions of eddy current density on the surfaces of the wires in case 1 (legend as in Figure 6): (a) Current density magnitude in wire 2; (b) current density in wire 1.

Line $m = 0$ (green) in Figure 6b corresponds to $J_1^{(0)}$ —the skin effect in wire 1. The first reaction to this current, $J_{2,1}^{(1)}$, is present in wire 2 (blue line $m = 1$ in Figure 6a). This reaction is quite large—the values are of the same order as $J_1^{(0)}$. It causes reaction $J_{1,2}^{(2)}$ in wire 1 (magenta line $m = 2$ in Figure 6b). Its value is several times smaller than $J_1^{(0)}$. Figure 6d shows that the values add in the vicinity of wire 2, whereas they subtract on the remaining surface of wire 1. It noticeably affects the current density in wire 1, which is best visible in Figure 7b, where the green line corresponds to $J_1^{(0)}$, the small magenta

shape in the center represents $J_{1,2}^{(2)}$, and the red line is the total current density in wire 1. The next reaction, $J_{2,1}^{(3)}$, generated in wire 2 is marked with yellow lines in Figure 6a,c (line $m = 3$). Its values are about 1% of the excitation in wire 1, therefore it marginally affects the current density in wire 2. This is visible in Figures 6a and 7a, where the total current density (red line) is practically the same as reaction 1. The next reactions are very small and can be completely neglected in this case.

It is noticeable that the first reaction in wire 2 due to current in wire 1 generates current density ($J_{2,1}^{(1)}$) of similar amplitude to the source current density in wire 1 ($J_1^{(0)}$), but the higher order reactions are much smaller. At first sight, this could seem a bit strange. However, it can be easily explained as follows: The first reaction eddy currents are generated by a non-zero total current in wire 1, whereas the total current in wire 2 remains zero. Mathematically speaking, the surface integral of current density $J_1^{(0)}$ in the first wire over its cross section is equal to current I_1 , whereas this kind of integral of current density $J_{2,1}^{(1)}$ over the cross section of the second wire equals zero. Therefore, the reaction due to the eddy currents is much smaller, because the eddy currents induced in wire 1 cancel partially due to opposing phases of $J_{2,1}^{(1)}$ in wire 2. In very large simplification, this is illustrated in Figure 8.

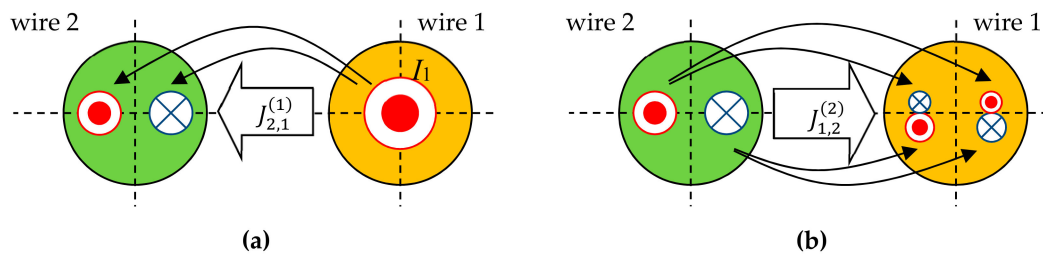


Figure 8. Symbolic illustration of reactions 1 and 2: (a) Reaction 1; (b) reaction 2.

Figure 9 shows the results for cases 2 and 3. Only results for wire 1 are shown, because the results for wire 2 are symmetrical. Reactions 0, 1, and 2 are shown (reactions 3 and higher are too small to be drawn together with reactions of lower order), as well as the total current density as the sum of the first six reactions. The results stay in agreement with the fact that the current density is shifted outwards in of same currents, whereas inwards in the case of opposing currents.

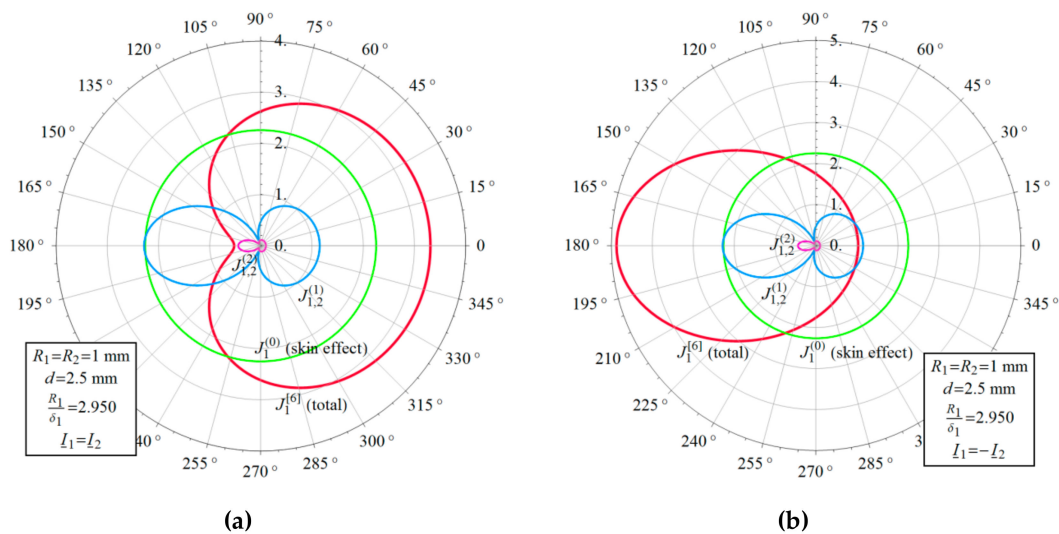


Figure 9. Polar plots of the relative current density magnitude on the surface of wire 1 (values in units of direct current density; legend: Red—total, green—skin effect, blue— $m = 1$, magenta— $m = 2$): (a) Case 2 (same currents); (b) case 3 (opposing currents).

The results can be compared with those obtained by means of finite elements. FEMM software (version 4.2, 64-bit 21Apr2019 by David Meeker, MA, USA, <http://www.femm.info/wiki/HomePage>) was used to perform the calculations with very dense mesh to ensure suitable accuracy, and Table 1 shows the results—the total current density at some specific points. The results agree very well—the differences in the magnitudes usually appear in the third meaningful digit, and the phase angles agree up to a degree.

Table 1. Comparison of the relative current density at specific points for the three cases solved by means of the proposed method and with use of FEMM software (magnitudes in units of uniform DC density, phases in degrees).

Point	Quantity	Case 1		Case 2		Case 3	
		Proposed	FEMM	Proposed	FEMM	Proposed	FEMM
$(R_1, 0^\circ)$	Magnitude	2.164	2.158	3.317	3.310	1.033	1.031
	Phase	38.3	37.9	41.5	41.3	27.6	27.0
$(R_1, 90^\circ)$	Magnitude	2.178	2.175	2.622	2.617	1.755	1.754
	Phase	37.5	37.1	42.0	41.7	30.8	30.3
$(R_1, 180^\circ)$	Magnitude	2.578	2.566	0.517	0.502	4.869	4.850
	Phase	46.7	47.1	-7.1	-6.2	51.7	51.8
$(R_2, 0^\circ)$	Magnitude	2.311	2.302	0.517	0.502	4.869	4.850
	Phase	-122.9	-122.8	-7.1	-6.3	-128.3	-128.2
$(R_2, 90^\circ)$	Magnitude	0.482	0.481	2.622	2.617	1.755	1.755
	Phase	62.7	62.8	42.0	41.7	-149.2	-149.7
$(R_2, 180^\circ)$	Magnitude	1.164	1.162	3.317	3.309	1.033	1.032
	Phase	47.7	47.6	41.5	41.3	-152.4	-153.0

3.2. Analysis of Function Λ

Function Λ , given by Equation (16), is crucial in the above considerations; therefore, it is worth investigating its behavior for various values of parameters. Figure 10 shows the values of Λ versus r/R at $R/d = 0.5$ for various θ and R/δ , where δ is the skin depth. It follows that the modulus is largest for $r = R$, which means the strongest reaction occurs on the wire surface. This is due to the fact that $I_n(\underline{r})$ analyzed in interval $0 \leq r \leq R$ has the largest modulus for $r = R$. Figure 11 shows Λ versus θ at for various R/d and R/δ . The largest modulus is for $\theta = 0$, because then $\cos n\theta = 1$ and all the terms in series (16) add together. This confirms that the strongest reaction occurs at the point closest to the source filament, as expected. The dependence of $|\Lambda|$ versus R/d and R/δ is shown in Figure 12. It follows that $|\Lambda|$ increases with an increase of both R/d and R/δ . Hence, the reactions are stronger the closer is the filament and the smaller is the skin depth.

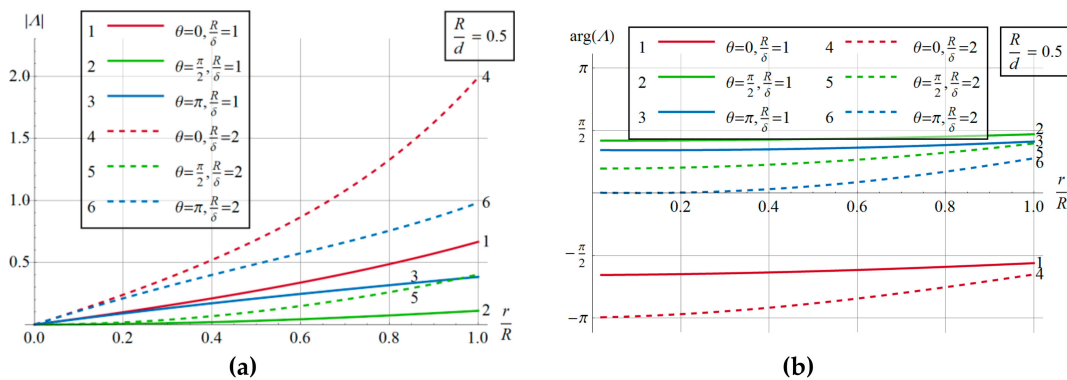


Figure 10. Values of Λ versus $\frac{r}{R}$ for $\theta = 0, \frac{\pi}{2}, \pi$ and $\frac{R}{\delta} = 1, 2$: (a) Modulus; (b) argument.

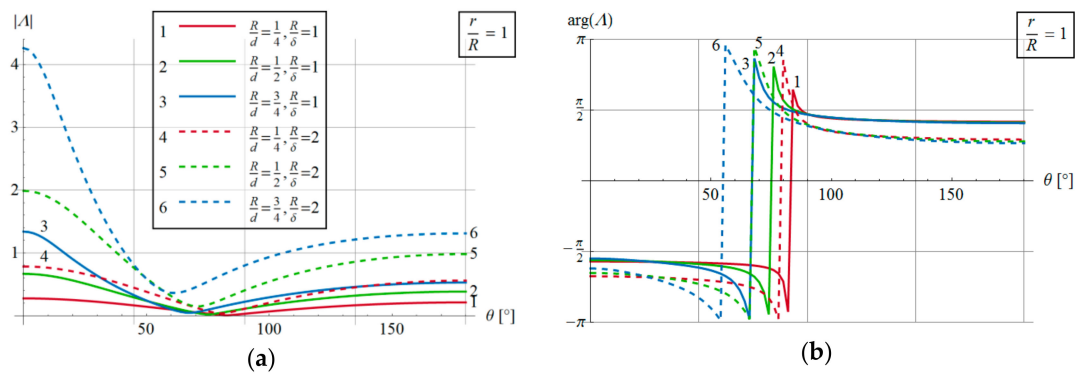


Figure 11. Values of Λ versus θ for $\frac{R}{d} = 0.25, 0.5, 0.75$ and $\frac{R}{\delta} = 1, 2$: (a) Modulus; (b) argument (legend as in (a)).

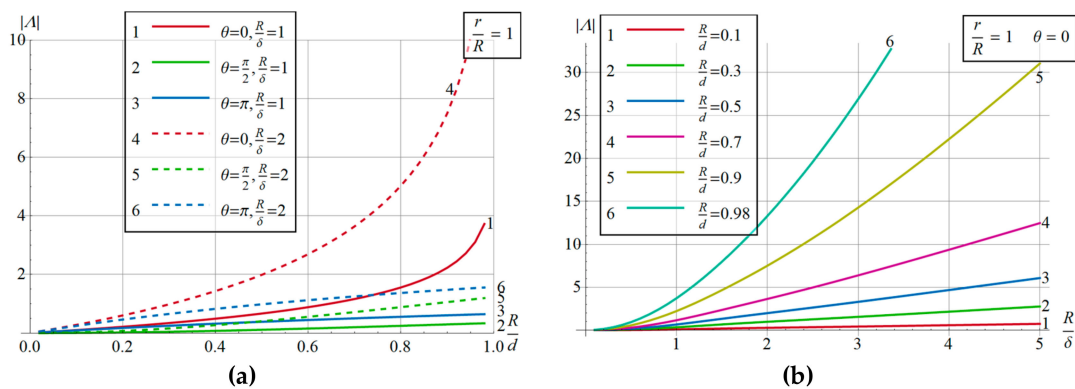


Figure 12. The dependence of $|\Lambda|$ versus the geometrical parameters and skin depth: (a) $|\Lambda|$ versus R/d ; (b) $|\Lambda|$ versus R/δ .

3.3. Analysis of the Successive Reactions

Let us consider an even reaction of current density in wire 1, i.e., $m = 2l$. By recursive applying Equation (19), it follows that

$$\mathbf{I}_{1,2}^{(2l)} = \Lambda_{1,2} \mathbf{I}_{2,1}^{(2l-1)} = \Lambda_{1,2} \Lambda_{2,1} \mathbf{I}_{1,2}^{(2l-2)} = \mathbf{I}_1 (\Lambda_{1,2} \Lambda_{2,1})^{l-1} \Lambda_{1,2} \Lambda_{2,1}. \quad (20a)$$

As for odd reactions, when $m = 2l - 1$, one obtains

$$\mathbf{I}_{1,2}^{(2l-1)} = \Lambda_{1,2} \mathbf{I}_{2,1}^{(2l-1)} = \Lambda_{1,2} \Lambda_{2,1} \mathbf{I}_{1,2}^{(2l-3)} = \mathbf{I}_2 (\Lambda_{1,2} \Lambda_{2,1})^{l-1} \Lambda_1. \quad (20b)$$

Similar equations can be obtained for wire 2. Hence, the even reactions in a wire only depend on the current in that wire, whereas the odd reactions depend on the current in the neighboring wire. Moreover, the modulus of each reaction only depends on current magnitudes and not their phases.

There are five parameters in Equation (17): Three geometrical sizes R_1, R_2, d , and two skin depths δ_1, δ_2 , which are related to material properties and frequency of currents. However, analysis of the Equations reveals that current density only depends on four ratios, $R_1/d, R_2/d, R_1/\delta_1, R_2/\delta_2$, which reduce to two parameters, R/d and R/δ , in case of two identical wires. Figure 13 shows the modulus of particular reactions of relative current density on the surface of wire 1 when the wires carry currents of the same r.m.s. value (of no matter what phases). It follows that the successive corrections are smaller and smaller—usually m th correction is several times smaller than the previous one. For a given reaction number, the reaction is the smaller the larger the gap between the wires, and the larger the smaller the skin depth. The influence of skin depth is significant—to obtain accuracy of three meaningful digits, it is enough to take three reactions for $\delta = R$, whereas four reactions may not be enough for $\delta = 0.5R$.

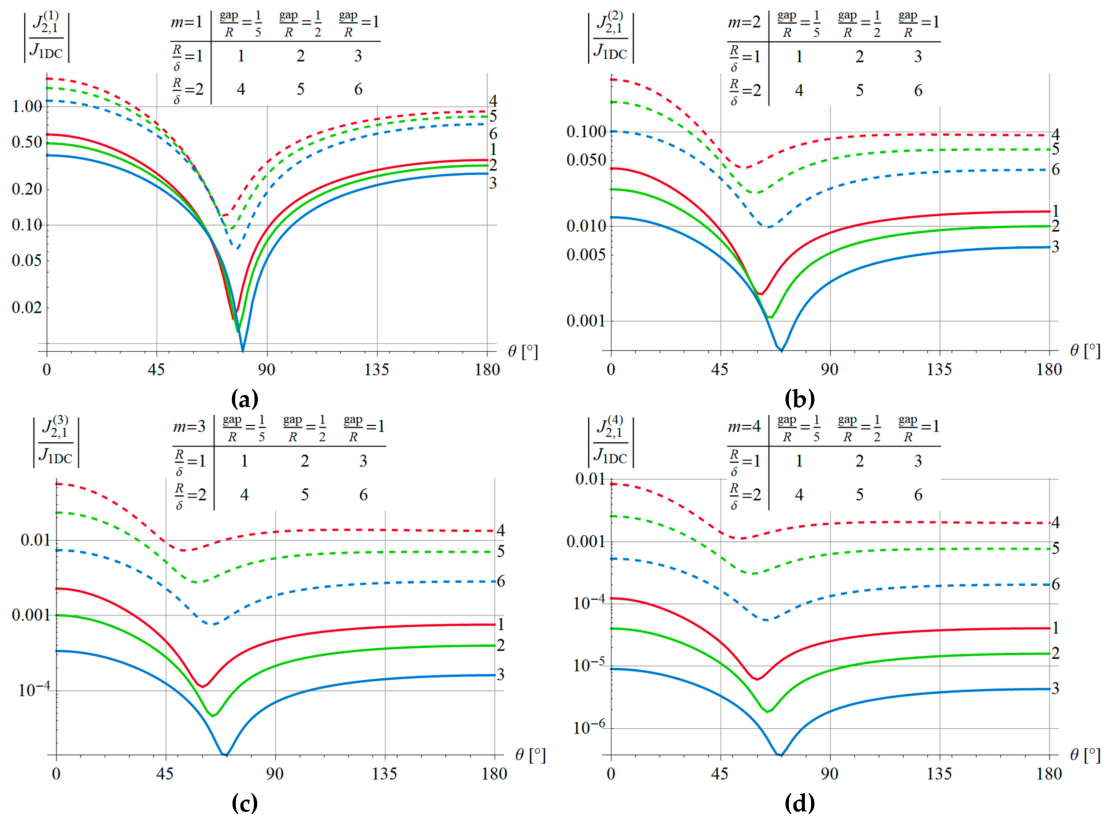


Figure 13. Modulus of several lower corrections to the relative current density in case of two identical wires of radius R for three gaps between them ($gap = d = -2R = 0.2R, 0.5R, R$) and two skin depths (R and $0.5R$): (a) Reaction 1; (b) reaction 2; (c) reaction 3; (d) reaction 4.

3.4. The Proximity Effect

Let us consider the proximity effect for two identical wires in two cases: (1) With the same currents in the wires (magnitude and phase), and (2) with opposing currents of equal magnitudes. As mentioned in Section 3.3, the corresponding even reactions are identical in both cases, whereas the corresponding odd reactions have opposing phases with the same modules. Therefore, the total current density differs in both cases. Figure 14 shows the total relative current density in wire 2 in the two cases for various gaps between the wires and for two skin depths. Six reactions were taken into account. In accordance with classical results, in case 1, the current density is shifted outwards, whereas in case 2, inwards. The effect is stronger the smaller the gap between the wires and the smaller the skin depth. It is worth noting that the effect is stronger for the case of opposing currents. This is best visible by comparing curves 1 and 4, 2 and 5, and 3 and 6 in Figure 14c,d, where the corresponding maximum values are larger for the case of opposing currents. It is also visible the current density at the wire center is not affected by the successive reactions—it remains the same as for the skin effect. Indeed, by analyzing Equations (16) and (17), it follows that all the successive corrections take a value of zero at the wire center.

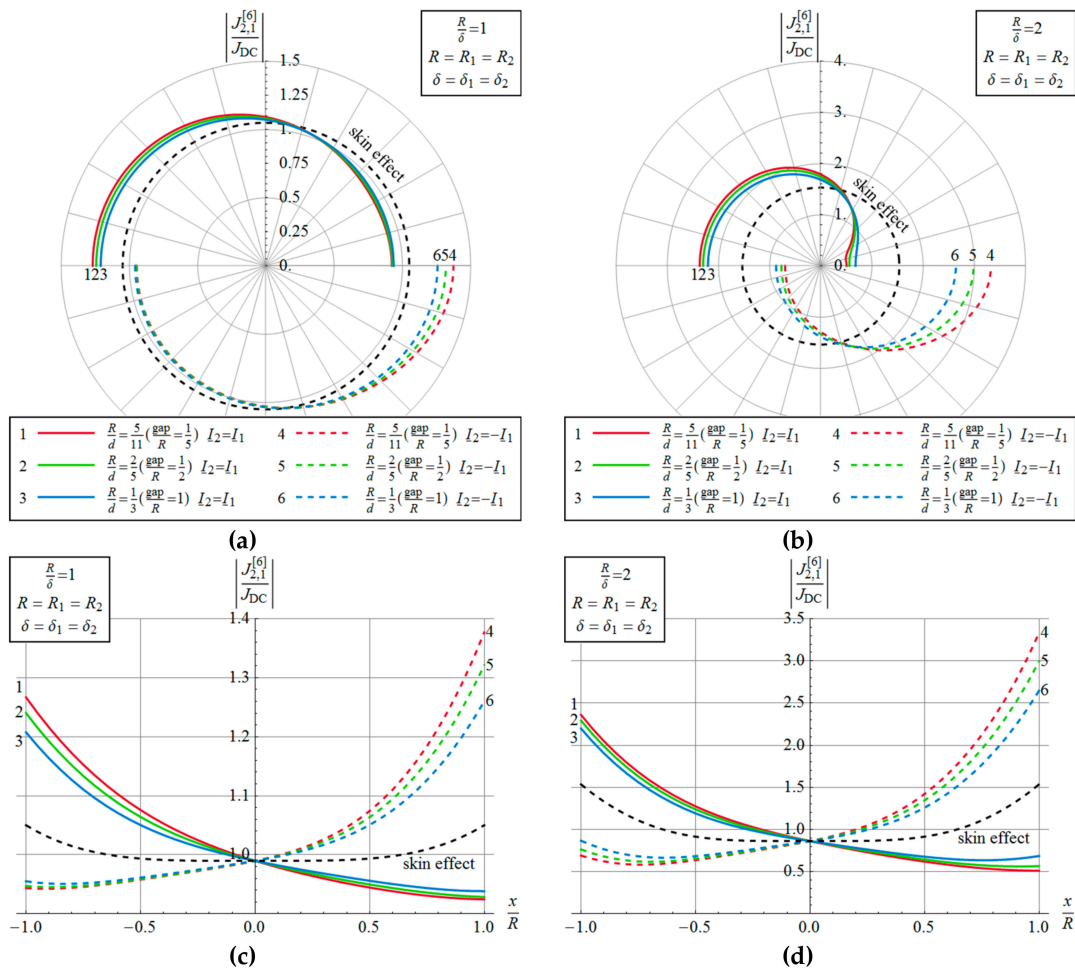


Figure 14. Polar plots of the modulus of the total relative current density in wire 2 for identical wires, various gaps between them and two skin depths (red, green, and blue lines correspond to different gaps between the wires; solid lines—same currents, dashed lines—opposing currents; black dashed line is for purely skin effect): (a) Values on surface at skin depth $\delta = R$; (b) values on surface at skin depth $\delta = 0.5R$; (c) values across the wire for skin depth $\delta = R$ (legend as in (a)); (d) values across the wire for skin depth $\delta = 0.5R$ (legend as in (b)).

4. Conclusions

The presented method of calculation of current density distribution is based on the method of successive reactions. It can be regarded as a semi-analytical one—while it allows obtaining analytical results for each current density reaction based on the previous one, it requires some kind of discretization. The following conclusions can be formulated:

- The results obtained show that there are four parameters directly affecting the current density: R_1/d , R_2/d , R_1/δ_1 , R_2/δ_2 , which facilitate further analysis.
- The corrections are artificial quantities that can be interpreted as reactions to currents due to previous corrections. They are just auxiliary quantities and cannot be measured—only their total is a real physical quantity.
- In the case of large enough skin depths, reactions 2 and higher can often be neglected without significant loss of accuracy. Therefore, the results with the first correction only are often accurate enough.
- The current density in the wire center is not affected by the corrections—it originates only from the skin effect.

- The current density of an even reaction in a wire is directly proportional to the current in that wire, whereas odd reactions are directly proportional to the current in the neighboring wire.
- The method is not without drawbacks—it cannot be used for non-circular wires and it requires discretization into segments, which introduces uncertainty.
- Further directions of the research can be generalization for a group of more than two wires, for tubular wires, or for wires in conductive environments.

Author Contributions: Conceptualization, Z.P. and P.J.; Methodology, Z.P. and P.J.; Software, P.J.; Validation, Z.P., D.K., and T.S.; Formal analysis, Z.P.; Writing—original draft preparation, Z.P. and P.J.; Writing—review and editing, D.K. and T.S.; Visualization, P.J. and Z.P.; Supervision, P.J.

Funding: This research received no external funding.

Conflicts of Interest: The authors declare no conflicts of interest.

Appendix A

Consider an infinitely long cylindrical conductor Ω of radius R , electric conductivity σ , and magnetic permeability μ placed in free space (μ_0). If a parallel infinitely long filament with time harmonic current of complex r.m.s. \underline{I} and angular frequency ω is placed at a distance of $d > R$, then eddy currents will be induced in the cylinder. Let us introduce a cylindrical coordinate system with z -axis located on the axis of the cylinder and x -axis crossing the filament (Figure A1).

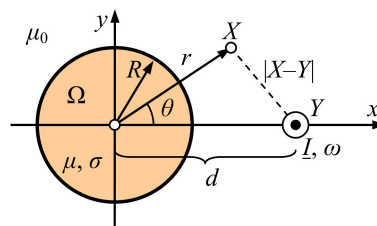


Figure A1. A long cylindrical conductor and a parallel current filament (cross section).

Due to geometrical conditions, currents flow along the z -axis; thus current density and vector magnetic potential only have z -components, which are independent on z -coordinate: $\underline{A} = \underline{A}(r, \theta)\hat{z}$ and $\underline{J} = \underline{J}(r, \theta)\hat{z}$. If $Y(d, 0)$ are coordinates of the filament, then the Maxwell equations lead to the following equations for the vector magnetic potential at point X :

$$\nabla^2 \underline{A}_{\text{in}}(X) - j\omega\mu\sigma \underline{A}_{\text{in}}(X) = 0 \quad \text{for } X \in \Omega, \quad (\text{A1})$$

$$\nabla^2 \underline{A}_{\text{out}}(X) - \mu_0 \underline{I} \delta(X - Y) \quad \text{for } X \notin \Omega. \quad (\text{A2})$$

where $\delta(X - Y)$ is the Dirac delta here. The potential outside the cylinder can be expressed as $\underline{A}_{\text{out}} = \underline{A}_{\text{react}} + \underline{A}_{\text{exc}}$, where $\underline{A}_{\text{react}}$ satisfies the Laplace equation, and

$$\underline{A}_{\text{exc}}(X) = \frac{\mu_0 \underline{I}}{2\pi} \ln \frac{1}{|X - Y|} + \underline{A}_0, \quad (\text{A3})$$

where \underline{A}_0 is freely assumed constant, and $|X - Y|$ represents the distance between points X and Y . The equations for $\underline{A}_{\text{in}}$ and $\underline{A}_{\text{react}}$ can be rewritten as follows:

$$\frac{1}{r} \frac{\partial}{\partial r} \left(r \frac{\partial \underline{A}_{\text{in}}}{\partial r} \right) + \frac{1}{r^2} \frac{\partial^2 \underline{A}_{\text{in}}}{\partial \theta^2} - \underline{I}^2 \underline{A}_{\text{in}} = 0, \quad (\text{A4})$$

$$\frac{1}{r} \frac{\partial}{\partial r} \left(r \frac{\partial \underline{A}_{\text{react}}}{\partial r} \right) + \frac{1}{r^2} \frac{\partial^2 \underline{A}_{\text{react}}}{\partial \theta^2} = 0, \quad (\text{A5})$$

where $\underline{\Gamma}^2 = j\omega\mu\sigma$. They can be easily solved via the method of separation of variables. Due to symmetry ($\underline{A}(r, -\theta) = \underline{A}(r, \theta)$) and finite field for $r = 0$, the solutions take the following forms:

$$\underline{A}_{\text{in}} = \sum_{n=0}^{\infty} C_n I_n(\underline{\Gamma}r) \cos n\theta, \quad (\text{A6})$$

$$\underline{A}_{\text{react}} = D_{01} + D_{02} \ln \frac{1}{r} + \sum_{n=1}^{\infty} D_n \left(\frac{R}{r}\right)^n \cos n\theta. \quad (\text{A7})$$

$\underline{A}_{\text{react}}$ should vanish for $r \rightarrow \infty$, because far from the cylinder, the field should remain unaffected; thus, $D_{01} = D_{02} = 0$. On boundary $r = R$, the equations of field continuity yield:

$$\underline{A}_{\text{in}} = \underline{A}_{\text{react}} + \underline{A}_{\text{exc}}, \quad \frac{1}{\mu} \frac{\partial \underline{A}_{\text{in}}}{\partial r} = \frac{1}{\mu_0} \frac{\partial (\underline{A}_{\text{react}} + \underline{A}_{\text{exc}})}{\partial r}. \quad (\text{A8})$$

To fulfill them, it is necessary to represent $\underline{A}_{\text{exc}}$ in terms of coordinates r and θ . By the cosine theorem it follows that (see Figure A1)

$$|X - Y|^2 = r^2 + d^2 - 2rd \cos \theta. \quad (\text{A9})$$

Hence

$$\ln \frac{1}{|X - Y|} = -\frac{1}{2} \ln(r^2 + d^2 - 2rd \cos \theta) = -\ln d - \frac{1}{2} \ln \left(1 + \left(\frac{r}{d}\right)^2 - 2\frac{r}{d} \cos \theta \right). \quad (\text{A10})$$

Then, by using Equation 1.514 from [28], which is

$$\ln(1 + x^2 - 2x \cos \theta) = -2 \sum_{n=1}^{\infty} \frac{1}{n} x^n \cos \theta, \quad |x| < 1, \quad (\text{A11})$$

one obtains

$$\ln \frac{1}{|X - Y|} = \sum_{n=1}^{\infty} \frac{1}{n} \left(\frac{r}{d}\right)^n \cos \theta - \ln d \quad (\text{A12})$$

so that

$$\underline{A}_{\text{exc}}(r, \theta) = \frac{\mu_0 I}{2\pi} \sum_{n=1}^{\infty} \frac{1}{n} \left(\frac{r}{d}\right)^n \cos \theta + \underline{A}_0 - \frac{\mu_0 I}{2\pi} \ln d \quad (\text{A13})$$

provided that $r < d$. It is convenient to set $\underline{A}_0 = \frac{\mu_0 I}{2\pi} \ln d$ to simplify the solution. Then Equation (A8) yields

$$C_0 = 0, \quad C_n = \frac{\mu_0 I}{2\pi} \left(\frac{R}{d}\right)^n \frac{2}{n I_n(\underline{\Gamma}R) + \frac{1}{\mu_r} \underline{\Gamma} R I_n'(\underline{\Gamma}R)}, \quad D_n = C_n I_n(\underline{\Gamma}R) - \frac{\mu_0 I}{2\pi} \frac{1}{n} \left(\frac{R}{d}\right)^n \quad (\text{A14})$$

For a non-magnetic cylinder ($\mu_r = 1$), C_n can be simplified by using the following recurrence relation for the modified Bessel functions (see Equation 8.486, position 3 in [28]):

$$n I_n(z) + z I_n'(z) = z I_{n-1}(z). \quad (\text{A15})$$

This leads to

$$C_n = \frac{\mu_0 I}{2\pi} \left(\frac{R}{d}\right)^n \frac{2}{\underline{\Gamma} R I_{n-1}(\underline{\Gamma}R)}, \quad (\text{A16})$$

so that

$$\underline{A}_{\text{in}}(r, \theta) = \frac{\mu_0 I}{\pi \underline{\Gamma} R} \sum_{n=1}^{\infty} \left(\frac{R}{d}\right)^n \frac{I_n(\underline{\Gamma}r)}{I_{n-1}(\underline{\Gamma}R)} \cos n\theta. \quad (\text{A17})$$

Finally, the eddy currents density inside the non-magnetic cylinder can be found as follows:

$$J_{\text{in}}(r, \theta) = -j\omega\sigma\Lambda_{\text{in}}(r, \theta) = -\frac{I}{\pi R^2} \Gamma R \sum_{n=1}^{\infty} \left(\frac{R}{d}\right)^n \frac{I_n(\Gamma r)}{I_{n-1}(\Gamma R)} \cos n\theta. \quad (\text{A18})$$

Appendix B

Function Λ , given by Equation (16), is essential in the whole procedure. In numerical calculations, the infinite series must be truncated to finite number of terms. To assure an accuracy of a meaningful digits in Λ , the series was cut at term $n = n_{\text{max}}$, for which the magnitude of $\left(\frac{R}{d}\right)^n \frac{I_n(\Gamma r)}{I_{n-1}(\Gamma R)}$ is not larger than the magnitude of the sum of lower order terms multiplied by a “small” number $\epsilon = 10^{-a}$. Figure A2 shows the number of required terms to obtain an accuracy of a digits for various values of the remaining parameters. It follows that:

- To obtain an accuracy of three significant digits, the number of terms, n_{max} , is up to several tens;
- n_{max} depends on angle and reaches the highest value for $\theta < 90^\circ$;
- n_{max} grows with increasing r and reaches maximum at $r = 1$;
- n_{max} grows with decreasing d ; and
- n_{max} usually grows with decreasing δ , but surprisingly not for all angles.

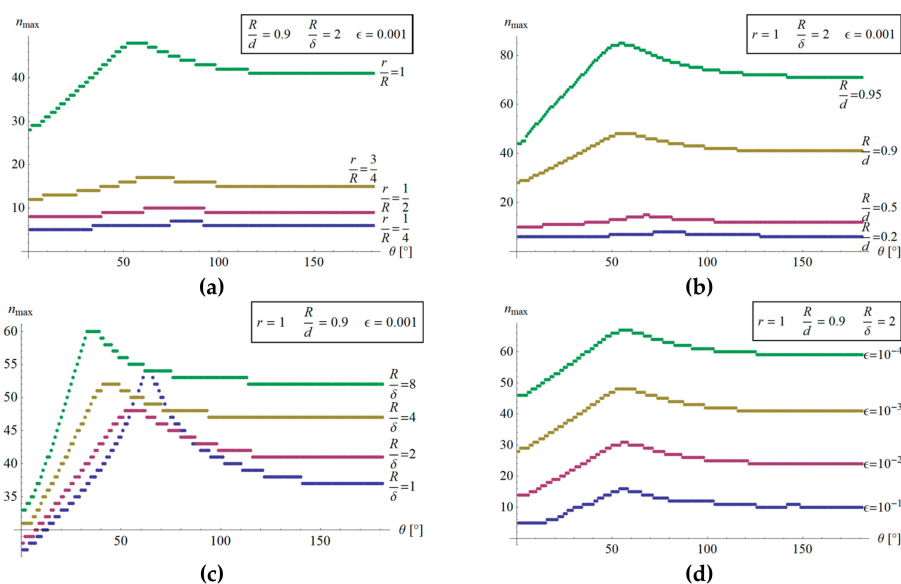


Figure A2. Number of terms in Equation (16) to obtain required accuracy versus angle θ : (a) For various $\frac{r}{R}$; (b) for various $\frac{R}{d}$; (c) for various $\frac{R}{\delta}$; (d) for various ϵ .

References

1. Benato, R.; Paoluci, A. *EHV AC Undergrounding Electrical Power. Performance and Planning*; Springer: London, UK, 2010.
2. Coufal, O. Current density in two solid parallel conductors and their impedance. *Electr. Eng.* **2014**, *96*, 287–297. [CrossRef]
3. Capelli, F.; Riba, J.R. Analysis of Equations to calculate the AC inductance of different configurations of nonmagnetic circular conductors. *Electr. Eng.* **2017**, *99*, 827–837. [CrossRef]
4. Pagnetti, A.; Xemard, A.; Pladian, F.; Nucci, C.A. An improved method for the calculation of the internal impedances of solid and hollow conductors with inclusion of proximity effect. *IEEE Trans. Power Deliv.* **2012**, *27*, 2063–2072. [CrossRef]
5. Cirino, A.W.; de Paula, H.; Mesquita, R.C.; Saraiva, E. Cable parameter determination focusing on proximity effect inclusion using finite element analysis. In Proceedings of the 2009 Brazilian Power Electronics Conference, Bonito (MS), Brasil, 27 September–1 October 2009; pp. 402–409. [CrossRef]

6. Dwight, H.B. Proximity effect in wires and thin tubes. *Trans. Am. Inst. Electr. Eng.* **1923**, *42*, 850–859. [[CrossRef](#)]
7. Piątek, Z. Method of calculating eddy currents induced by the sinusoidal current of the parallel conductor in the circular conductor. *ZN Pol. Śl. Elektryka* **1981**, *75*, 137–150.
8. Piątek, Z. *Impedances of Tubular High Current Busducts*; Polish Academy of Sciences: Warsaw, Poland, 2008.
9. Jabłoński, P. Cylindrical conductor in an arbitrary time-harmonic transverse magnetic field. *Prz. Elektrotech.* **2011**, *87*, 49–53.
10. Filipović, D.; Dlabac, T. Closed Form Solution for the Proximity Effect in a Thin Tubular Conductor Influenced by a Parallel Filament. *Serb. J. Electr. Eng.* **2010**, *7*, 13–20. [[CrossRef](#)]
11. Payne, A. Skin Effect, Proximity Effect and the Resistance of Circular and Rectangular Conductors. ©Alan Payne. 2017. Available online: <http://g3rbj.co.uk/wp-content/uploads/2017/06/Skin-Effect-Proximity-Loss-and-the-Resistance-of-Circular-and-Rectangular-Conductors-Issue-4.pdf> (accessed on 21 July 2019).
12. Riba, J.R. Analysis of Equations to calculate AC resistance of different conductors' configurations. *Electr. Power Syst. Res.* **2015**, *127*, 93–100. [[CrossRef](#)]
13. Kim, J.; Park, Y.J. Approximate Closed-Form Equation for Calculating Ohmic Resistance in Coils of Parallel Round Wires With Unequal Pitches. *IEEE Trans. Ind. Electron.* **2015**, *62*, 3482–3489.
14. Aebischer, H.A.; Friedli, H. Analytical approximation for the inductance of circularly cylindrical two-wire transmission lines with proximity effect. *Adv. Electromagn.* **2018**, *7*, 25–34. [[CrossRef](#)]
15. Dlabac, T.; Filipović, D. Integral equation approach for proximity effect in a two-wire line with round conductors. *Tech. Vjesn.* **2015**, *22*, 1065–1068. [[CrossRef](#)]
16. Filipović, D.; Dlabac, T. Proximity effect in a shielded symmetrical three-phase line. *Serb. J. Electric. Eng.* **2014**, *11*, 585–596. [[CrossRef](#)]
17. Brito, A.; Maló Machado, V.; Almeida, M.E.; Guerreiro das Neves, M. Skin and Proximity Effects in the Series-Impedance of Three-Phase Underground Cables. *Electr. Power Syst. Res.* **2016**, *130*, 132–138. [[CrossRef](#)]
18. Riba, J.R. Calculation of AC to DC resistance ratio of conductive nonmagnetic straight conductors by applying FEM simulations. *Eur. J. Phys.* **2015**, *36*, 055019. [[CrossRef](#)]
19. Riba, J.R.; Capelli, F. Calculation of the inductance of conductive nonmagnetic conductors by means of finite element method simulations. *Int. J. Electr. Educ.* **2018**, *13*, 1–23. [[CrossRef](#)]
20. Jabłoński, P. Approximate BEM analysis of time-harmonic magnetic field due to thin-shielded wires. *Poznan Univ. Technol. Acad. J. Electr. Eng.* **2012**, *69*, 57–64.
21. Shendge, A. A study on a conductor system for investigation of proximity effect. *J. Electromagn. Anal. Appl.* **2012**, *4*, 440–446. [[CrossRef](#)]
22. Piątek, Z. Self and mutual impedances of a finite length gas-insulated transmission line (GIL). *Electr. Power Syst. Res.* **2007**, *77*, 191–201. [[CrossRef](#)]
23. Piątek, Z.; Kusiak, D.; Szczegielniak, T. Electromagnetic field and impedances of high current busducts. In Proceedings of the 2010 International Symposium, Wroclaw, Poland, 20–22 September 2010.
24. Rolicz, P. Eddy currents generated in a system of two cylindrical conductors by a transverse alternating magnetic field. *Electr. Power Syst. Res.* **2009**, *79*, 295–300. [[CrossRef](#)]
25. Piątek, Z.; Baron, B.; Jabłoński, P.; Kusiak, D.; Szczegielniak, T. Numerical method of computing impedances in shielded and unshielded three-phase rectangular busbar systems. *Prog. Electromagn. Res. B* **2013**, *51*, 135–156. [[CrossRef](#)]
26. Freitas, D.; Guerreiro das Neves, M.; Almeida, M.E.; Maló Machado, V. Evaluation of the Longitudinal Parameters of an Overhead Transmission Line with Non-Homogeneous Cross Section. *Electr. Power Syst. Res.* **2015**, *119*, 478–484. [[CrossRef](#)]
27. Moon, P.; Spencer, D.E. *Foundations of Electrodynamics*; D. Van Nostrand Company, Inc.: New York, NY, USA, 1960.
28. Gradshteyn, I.S.; Ryzhik, I.M. *Tables of Integrals, Sums, Series and Products*, 17th ed.; Elsevier Academic Press: Cambridge, MA, USA, 2007.

